Representation of Poloidal Asymmetries in Neoclassical Fluid Rotation Calculations in Axisymmetric Tokamaks

T. G. Collart – Georgia Tech

W. M. Stacey – Georgia Tech

Sherwood Theory Meeting 2015

NYU, New York, March 2015

Overview

In axisymmetric tokamaks the leading order “parallel” viscosity terms in the toroidal angular momentum damping term vanish identically on flux surface averaging, leaving the gyroviscous terms as the largest surviving viscous drag [3]. Since the gyroviscous terms depend on poloidal asymmetries, it is important to represent the poloidal variations in the plasma geometry accurately. In the interests of improving this poloidal representation, this analysis attempts to:

1. Develop an accurate method to analytically fit the poloidal and radial dependence of flux surfaces from EFIT data

2. Develop an orthogonal system of basis vectors and scale factors which allow for an accurate calculation of poloidal magnetic field

3. Solve a system of equations developed from the Fourier moments of the fluid equations for the poloidal asymmetries in plasma parameters

References

[1] Braginskii, Rev. Plasma Phys. Vol. 1, 205 (1965)
[3] W.M. Stacey and D.J. Sigmar, Phys. Fluids **28**, 9 (1985)
[2] W.M. Stacey, A. W. Bailey, D.J. Sigmar, and K.C. Shaing, Nucl. Fusion **25**, 463 (1985)
[5] R.L. Miller, M.S. Chu, J.M. Greene, Y.R. Lin-Liu, and R.E. Waltz, Phys. of Plasmas **5**, 973 (1998)
[6] J. Candy, Plasma Phys. Control. Fusion **51**, (2009) 105009
[7] W.M. Stacey, R.W. Johnson, and J. Mandrekas, Phys. of Plasmas **13**, 062508 (2006)
[8] C. Bae, W.M. Stacey and W.M. Solomon, Nucl. Fusion **53** (2013) 043011

Fluid moments of the Boltzmann Transport Equation

- Continuity

$$\frac{\partial n_i}{\partial t} + \nabla \cdot \left(n_i \vec{V}_i \right) = S_i^0$$

- Momentum Balance

$$\frac{\partial}{\partial t}\left[m_i n_i \vec{V}_i \right] + \nabla \cdot \overleftrightarrow{M}_i = n_i e_i \left(\vec{E} + \vec{V}_i \times \vec{B} \right) + \vec{F}_i^1 + \vec{S}_i^1$$

$$\overleftrightarrow{M}_i = n_i m_i \vec{V}_i \vec{V}_i + \overleftrightarrow{I} P_i + \overleftrightarrow{\Pi}_i$$

Viscosity and Friction

- The viscous stress tensor in a magnetized plasma can be decomposed into parallel, perpendicular, and gyroviscous components [1,2]

$$\overleftrightarrow{\Pi}_i = \overleftrightarrow{\Pi}_i^0 + \overleftrightarrow{\Pi}_i^{12} + \overleftrightarrow{\Pi}_i^{34}$$

- Each component of the stress tensor has an associated viscosity coefficient:

$$\eta_0 \simeq nT\tau \gg \eta_{3,4} \simeq \frac{nT\tau}{\Omega\tau} \gg \eta_{1,2} \simeq \frac{nT\tau}{(\Omega\tau)^2}$$

- In this analysis, we use a banana-plateau – PS viscosity interpolation formula to replace the parallel viscosity coefficient [3]

$$\eta_{0i} = 2n_i T_i \left(\frac{qR_0}{\bar{V}_{thi}} \frac{\epsilon^{-3/2}\nu_{ii}^*}{\left(1+\epsilon^{-3/2}\nu_{ii}^*\right)\left(1+\nu_{ii}^*\right)} \right)$$

- The interspecies frictional force is represented using a simple Lorentz model, with a collision frequency given by: [3]

$$\bar{\nu}_{\alpha,\beta} = \frac{1}{6\sqrt{2}\,\pi^{3/2}\epsilon_0^2} \frac{n_\beta e_\alpha{}^2 e_\beta{}^2 \sqrt{\mu_{\alpha,\beta}}\, ln\Lambda}{m_\alpha T^{3/2}}$$

Methods of analytically representing the variations in flux surface locations

- **Extended Miller –** Miller et. al. [5] gives the following expressions for major radius (R) and vertical displacement (Z) of points on flux surfaces, parameterized by constant ρ (normalized minor radius on outboard midplane). *We extend this application to include separate upper and lower hemisphere radial profiles of elongations* $(\delta[\rho])$ *and triangularities* $(\kappa[\rho])$:

$$R[\rho,\theta] = R_0[r] + a[\rho]\cos\left[\xi[\rho,\theta]\right]$$
$$Z[\rho,\theta] = Z_0[r] + a[\rho]\kappa[\rho]\sin[\theta]$$

$$\xi[\rho,\theta] = \theta + \arcsin\left[\delta[\rho]\right]\sin[\theta]$$

- **r-Fourier** - If a Fourier expansion is used to describe the poloidal dependence of the minor radius*, the poloidal dependence of R and Z can be written as:

$$R[\rho,\theta] = R_0[r] + r[\rho,\theta]\cos[\theta]$$
$$Z[\rho,\theta] = Z_0[r] + r[\rho,\theta]\sin[\theta]$$

$$r[\rho,\theta] = \bar{r}[\rho] + \sum_{i=1}^{n}\left(r_i^s[\rho]\sin[i\theta] + r_i^c[\rho]\cos[i\theta]\right)$$

* Note that a 0^{th} order expansion in r-Fourier results in the circular-model plasma representation

General Plasma Coordinate System

- The definitions for R and Z in both of the coordinate systems analyzed in this analysis can be used to derive the general basis vectors and scale factors, in terms of radial (ρ) and poloidal (θ) gradients. The poloidal basis vectors are parallel to flux-surfaces.
- In a general plasma coordinate system, the radial and poloidal basis vectors are not necessarily orthogonal.

Covariant Basis Vectors

$$\hat{g}_\rho = \frac{\partial R}{\partial \rho}\hat{e}_R + \frac{\partial Z}{\partial \rho}\hat{e}_Z$$

$$\hat{g}_\theta = \frac{\partial R}{\partial \theta}\hat{e}_R + \frac{\partial Z}{\partial \theta}\hat{e}_Z$$

$$\hat{g}_\phi = R\hat{e}_T$$

Scale Factors

$$h_{\rho\rho} = h_\rho = \sqrt{\left(\frac{\partial R}{\partial \rho}\right)^2 + \left(\frac{\partial Z}{\partial \rho}\right)^2}$$

$$h_{\theta\theta} = h_\theta = \sqrt{\left(\frac{\partial R}{\partial \theta}\right)^2 + \left(\frac{\partial Z}{\partial \theta}\right)^2}$$

$$h_{\phi\phi} = h_\phi = R$$

$$h_{\rho\theta} = h_{\theta\rho} = \frac{\partial R}{\partial \rho}\frac{\partial R}{\partial \theta} + \frac{\partial Z}{\partial \rho}\frac{\partial Z}{\partial \theta}$$

$$H_{\rho\theta} = \frac{\partial R}{\partial \rho}\frac{\partial Z}{\partial \theta} - \frac{\partial R}{\partial \theta}\frac{\partial Z}{\partial \rho} > 0$$

Metric Tensors

$$g_{ij} = \begin{pmatrix} h_{\rho\rho}{}^2 & h_{\theta\rho}{}^2 & 0 \\ h_{\theta\rho}{}^2 & h_{\theta\theta}{}^2 & 0 \\ 0 & 0 & h_{\phi\phi}{}^2 \end{pmatrix}$$

$$g^{ij} = \frac{1}{H_{\rho\theta}{}^2}\begin{pmatrix} h_{\theta\theta}{}^2 & -h_{\rho\theta}{}^2 & 0 \\ -h_{\theta\rho}{}^2 & h_{\rho\rho}{}^2 & 0 \\ 0 & 0 & H_{\rho\theta}{}^2 h_{\phi\phi}{}^{-2} \end{pmatrix}$$

Orthogonalized Plasma Coordinate System

- In the interest of simplifying vector calculations in the fluid equations, we can develop "orthogonalized" coordinate systems, by applying a method similar to a Grahm-Schmidt orthogonalization to the metric tensor.
- Effectively, we define a new radial basis vector which is perpendicular to both the toroidal and poloidal basis vectors, and is scaled to preserve the differential volume $\mathrm{d}V = H_{\rho\theta} h_{\phi}\, \mathrm{d}\rho\, \mathrm{d}\theta\, \mathrm{d}\phi$ from the general coordinate systems

Covariant Basis Vectors

$$\left(\hat{g}_{\rho}\right)^{\perp} = \frac{H_{\rho\theta}}{h_{\theta}^{f\,2}} \left(\frac{\partial Z}{\partial \theta} \hat{e}_R - \frac{\partial R}{\partial \theta} \hat{e}_Z \right)$$

$$\left(\hat{g}_{\theta}\right)^{\perp} = \left(\frac{\partial R}{\partial \theta} \hat{e}_R + \frac{\partial Z}{\partial \theta} \hat{e}_Z \right)$$

$$\left(\hat{g}_{\phi}\right)^{\perp} = R \hat{e}_T$$

Scale Factors

$$\left(h_{\rho\rho}\right)^{\perp} = \frac{\left(\frac{\partial R}{\partial \rho} \frac{\partial Z}{\partial \theta} - \frac{\partial R}{\partial \theta} \frac{\partial Z}{\partial \rho} \right)}{\sqrt{\left(\frac{\partial R}{\partial \theta} \right)^2 + \left(\frac{\partial Z}{\partial \theta} \right)^2}}$$

$$\left(h_{\theta\theta}\right)^{\perp} = h_{\theta} = \sqrt{\left(\frac{\partial R}{\partial \theta} \right)^2 + \left(\frac{\partial Z}{\partial \theta} \right)^2}$$

$$\left(h_{\phi\phi}\right)^{\perp} = h_{\phi} = R$$

$$\left(h_{\rho\theta}\right)^{\perp} = 0$$

Metric Tensors

$$\left(g_{ij}\right)^{\perp} = \begin{pmatrix} H_{\rho\theta}{}^{2} h_{\theta}^{-2} & 0 & 0 \\ 0 & h_{\theta}^{2} & 0 \\ 0 & 0 & R^2 \end{pmatrix}$$

$$\left(g^{ij}\right)^{\perp} = \begin{pmatrix} h_{\theta}^{2} H_{\rho\theta}^{-2} & 0 & 0 \\ 0 & h_{\theta}^{-2} & 0 \\ 0 & 0 & R^{-2} \end{pmatrix}$$

Method for fitting flux surfaces from EFIT data

- The location of flux-surfaces is determined for Shot # 149468 from a 65x65 (R,Z) mesh of EFIT data for the 2D poloidal magnetic flux (ψ) distribution over a poloidal plasma cross-section.
- The location of the plasma center is determined by the minimum ψ value, and the value of maximum ψ is determined by the location of the last-closed-flux surface.
- Flux-surface contours can be interpolated for 50 intermediate values of ψ. The central Z0 location for each of these surfaces is defined by the average vertical position of the locations of maximum and minimum major radii on the outboard and inboard midplanes. The R0 location for each flux-surface is determined by the midpoint between flux-surface boundaries at this point.
- The midplane minor radii for all flux surfaces is set by half the width of the flux-surface contours at the central (R0,Z0) location. Using the resulting relationship between flux surface ψ values and normalized midplane minor radii (ρ), we can interpolate to find 200 (R,Z) locations on flux-surface contours for each of 50 evenly-spaced ρ values, $0<\rho\leq 1$.

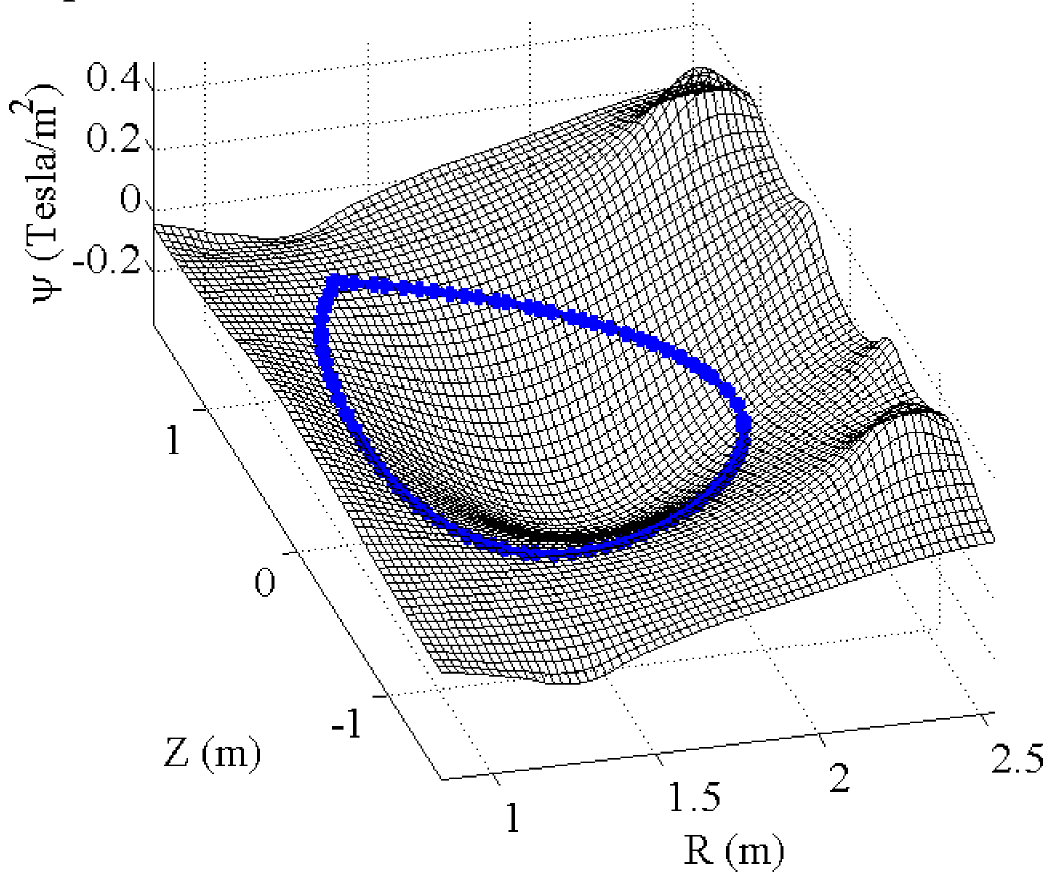

Figure – (R,Z) mesh of EFIT data for shot #149468. The location of the LCFS is shown in blue

0^{th} order r-Fourier (Circular Model) flux surface fitting

General and orthogonalized basis vector calculations for r-Fourier

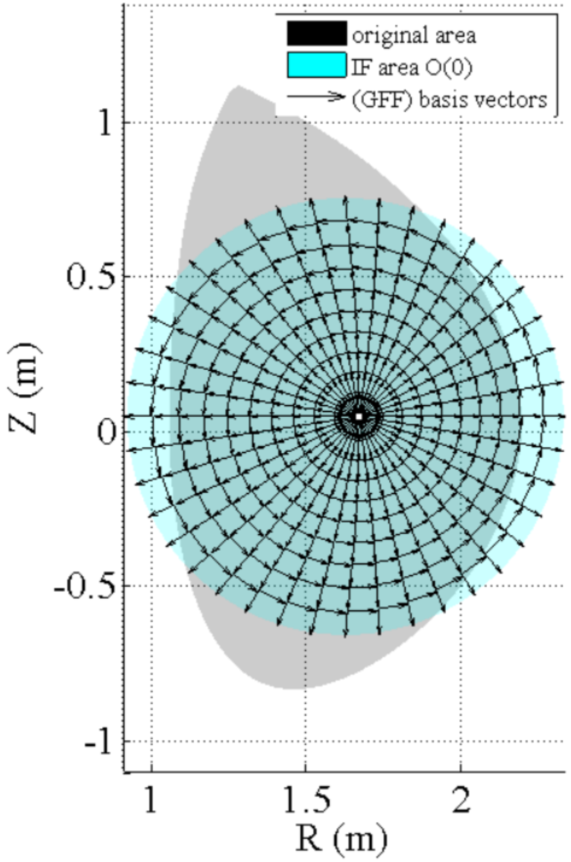

Left Plot:
Interpolated Fourier (IF) – Independent poloidal interpolation of Fourier fit coefficients on each flux surface (blue)
General Fitted Fourier* (GFF) – General, non-orthogonal basis vectors

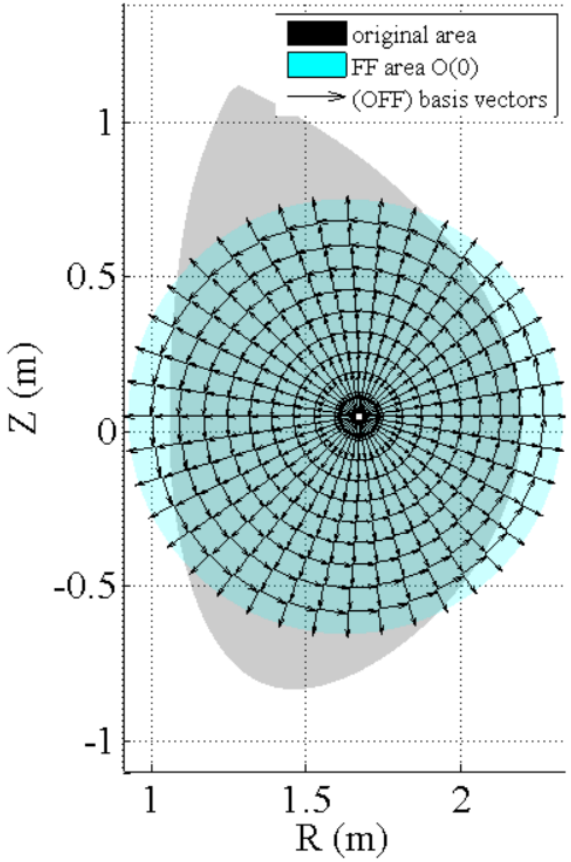

Right Plot:
Fitted Fourier (FF) – Reconstruction from 4^{th} order, piecewise polynomial fits of the radial dependence of Fourier coefficients
Orthogonalized Fitted Fourier* (OFF) – Orthogonalized basis vectors

A 0^{th} order Fourier expansion of the poloidal dependence of minor radius reduces to the circular-plasma model, with Shafranov shift:

$$R[\rho,\theta] = R_0[r] + \bar{r}[\rho]\cos[\theta]$$

$$Z[\rho,\theta] = Z_0[r] + \bar{r}[\rho]\sin[\theta]$$

This parameterization requires 3 radial profiles, and radial gradients:

$$\{R_0[\rho], Z_0[\rho], \bar{r}[\rho]\}$$

* For this simple circular model, the general and orthogonalized metric tensors are equivalent

6^{th} order r-Fourier model flux surface location fitting

General and orthogonalized basis vector calculations for r-Fourier

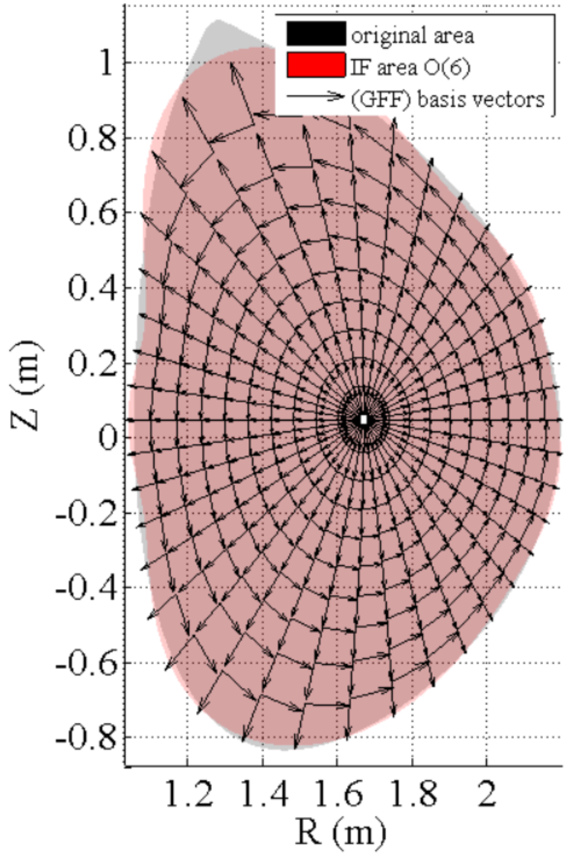

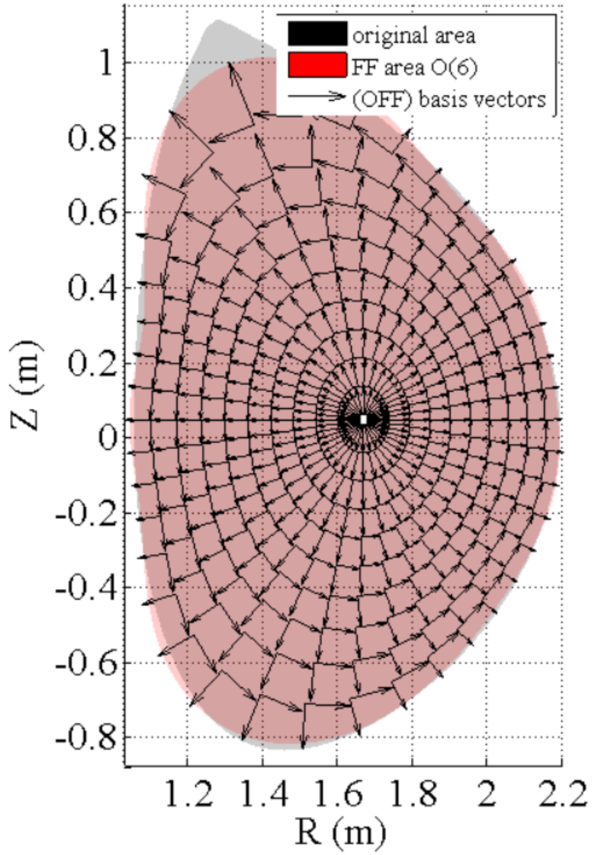

Reconstruction of the plasma area from a **6^{th} order Fourier fit** of the poloidal dependence of EFIT minor radius for flux surfaces **(red)**, as compared to the original **EFIT** plasma area **(grey)**.

$$R[\rho,\theta] = R_0[r] + \bar{r}[\rho]\cos[\theta]$$

$$Z[\rho,\theta] = Z_0[r] + \bar{r}[\rho]\sin[\theta]$$

$$r[\rho,\theta] = \bar{r}[\rho]$$

$$+\sum_{i=1}^{6}\left(r_i^s[\rho]\sin[i\theta] + r_i^c[\rho]\cos[i\theta]\right)$$

This parameterization requires 3 + 2n = 15 radial profiles, and radial gradients:

$$\left\{R_0[\rho], Z_0[\rho], \bar{r}[\rho], r_i^s[\rho], r_i^c[\rho]\right\}$$

Left Plot:

Interpolated Fourier (IF) – Independent poloidal interpolation of Fourier fit coefficients on each flux surface (blue)

General Fitted Fourier (GFF) – General, non-orthogonal basis vectors

Right Plot:

Fitted Fourier (FF) – Reconstruction from 6^{th} order, piecewise polynomial fits of the radial dependence of Fourier coefficients

Orthogonalized Fitted Fourier (OFF) – Orthogonalized basis vectors

Extended* Miller model flux-surface location fitting

General and orthogonalized basis vector calculations

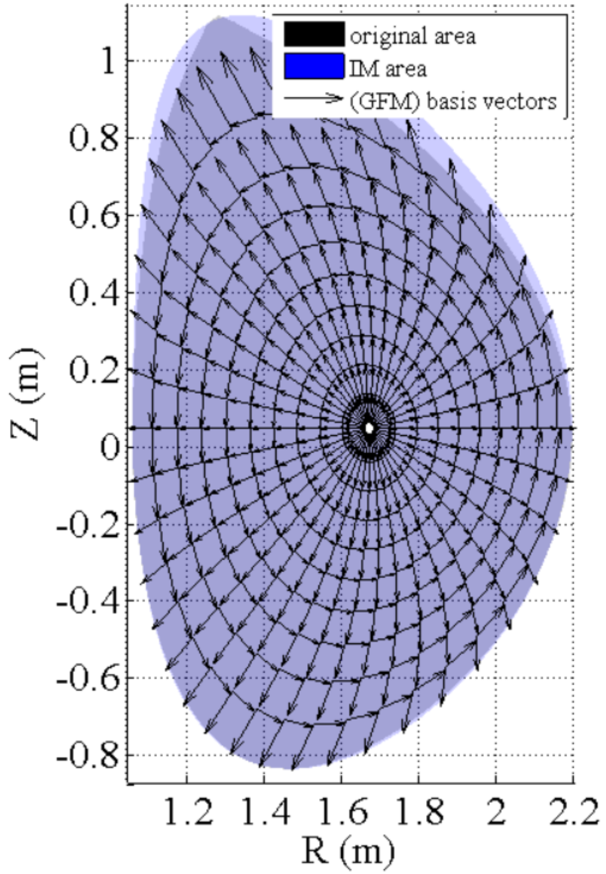

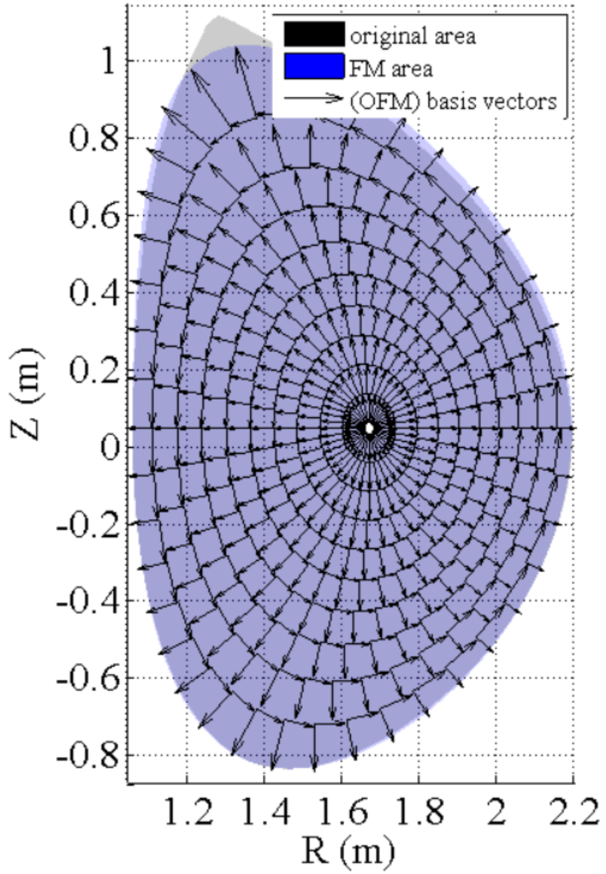

Left Figure:

Interpolated Miller (IM) – Independent poloidal interpolation of Miller parameters on flux surfaces (blue)

General Fitted Miller (GFM) – general, non-orthogonal basis vectors

Right Figure:

Fitted Miller (FM) – Reconstruction from 4th order, piecewise polynomial fits of the radial dependence of Miller parameters

Orthogonalized Fitted Miller (OFM) – orthogonalized basis vectors

Reconstruction of the poloidally-interpolated (*Left)* and fitted (*Right)* extended-Miller plasma areas (blue), as compared to the original EFIT plasma area (grey).

$$R[\rho,\theta] = R_0[r] + a[\rho]\cos[\xi[\rho,\theta]]$$

$$Z[\rho,\theta] = Z_0[r] + a[\rho]\kappa[\rho]\sin[\theta]$$

This parameterization requires 6 radial profiles, and radial gradients:

$$\left\{ \begin{matrix} R_0[\rho], Z_0[\rho], \\ \kappa_{up}[\rho], \kappa_{low}[\rho], \delta_{up}[\rho], \delta_{low}[\rho] \end{matrix} \right\}$$

* Separate radial elongation (κ) and triangularity (δ) profiles are used to fit the flux surfaces in the upper and lower hemispheres

The error in flux-surface interpolation and fitting methods, as compared to the original EFIT data

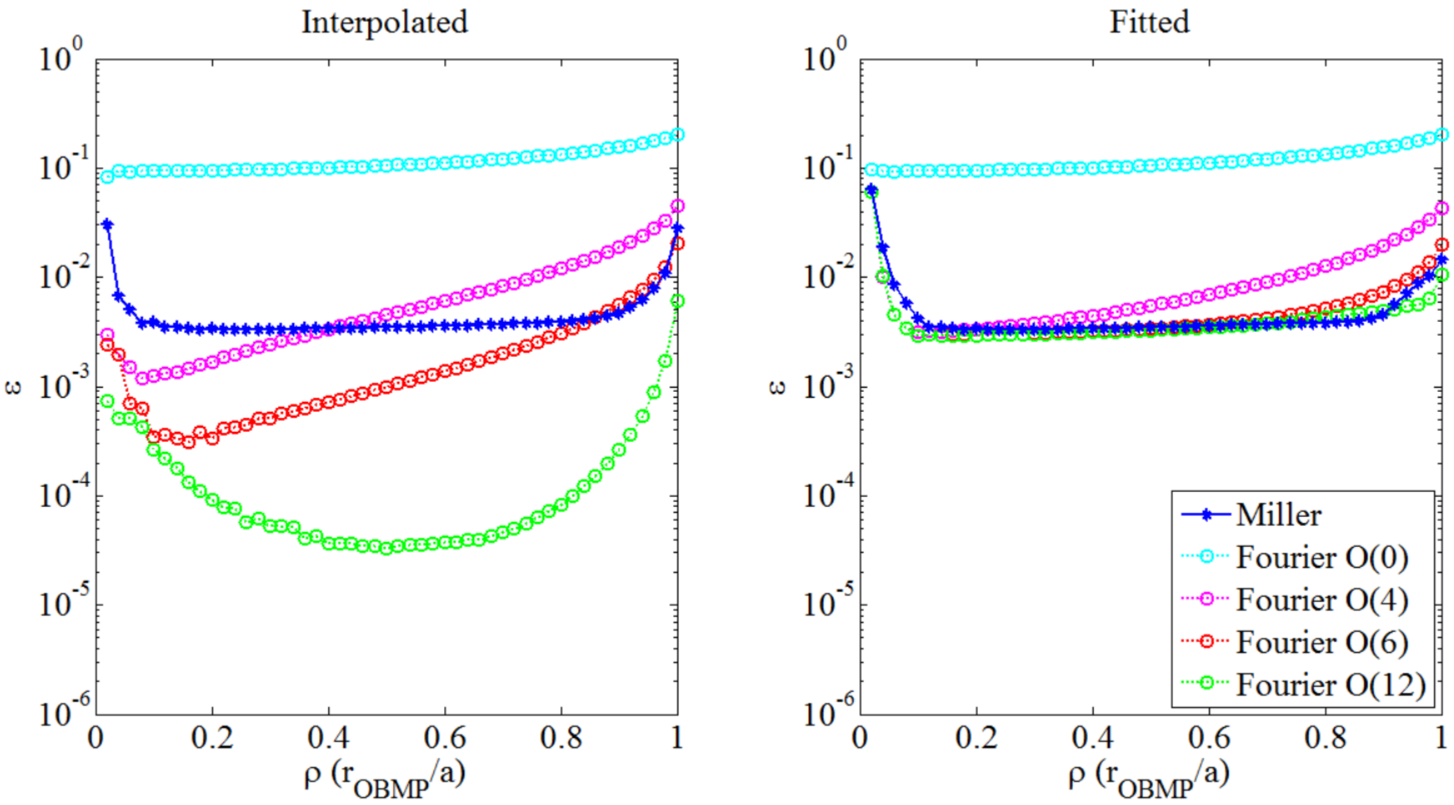

Error Calculation [6]:

$$\varepsilon = \frac{1}{n_\theta}\sum_{i=1}^{n_\theta}\frac{1}{r[\theta]}\sqrt{\left(R_i^{EFIT} - R[\theta_i]\right)^2 + \left(Z_i^{EFIT} - Z[\theta_i]\right)^2}$$

$n_\theta = 200$ (number of poloidal mesh points)

The Fitted extended-Miller model matches the EFIT flux surface with a relatively high accuracy (within 1% for rho<0.98), while also requiring ~ half as many radial profiles of fitting-coefficients as the r-Fourier model (6 vs 15)

In this analysis, we have chosen to use the **Fitted extended-Miller (FM)** plasma model to describe the flux surface locations, and the orthogonalization method to determine the basis vectors in this system. This model gives an analytic representation for both poloidal and radial variations in flux-surface location, and an analytic representation for basis vectors. It will be referred to as the **Orthogonalized Miller (OM)** model

The poloidal magnetic field is directly related to the plasma coordinates by spatial gradients of enclosed magnetic flux (ψ)

- The poloidal magnetic flux, magnetic field, and magnetic vector potential are related by [6]:

(1) $$\Phi_\theta = \int \vec{B} \cdot \mathrm{d}\vec{S}_\theta = 2\pi\psi$$

$$\vec{B} = \nabla \times \vec{A}$$

- **(1)** can be used to relate the poloidal magnetic field to R and Z gradients of ψ[R,Z]. Spline interpolations of the EFIT data can be used to calculate these gradients.

(2) $$B_{\theta,RZ} = \frac{1}{R}\sqrt{\left(\frac{\partial\psi}{\partial Z}\right)^2 + \left(\frac{\partial\psi}{\partial R}\right)^2}$$

- Following the same procedure, the poloidal field in terms of the flux-surface OM fits can be given in terms of only the radial gradient of ψ[ρ, θ], since the poloidal gradient vanishes:

(3) $$B_{\theta,\rho\theta} = \frac{1}{h_\rho R}\frac{\partial\psi}{\partial\rho}$$

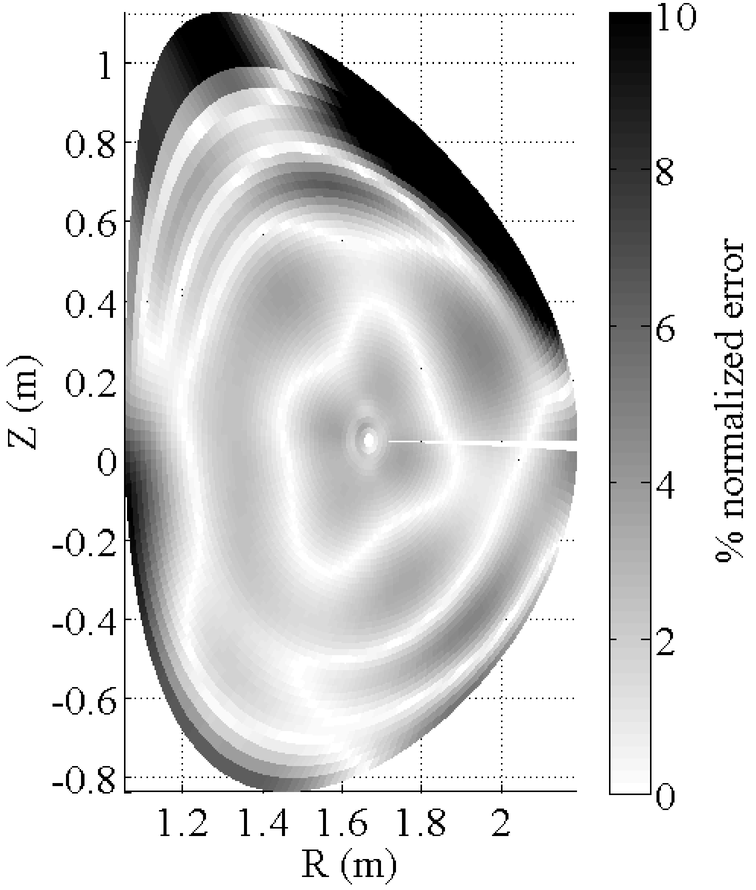

Figure – The normalized error between the calculations of poloidal magnetic field in the two coordinate systems

Comparison of EFIT and OM calculations of poloidal magnetic field

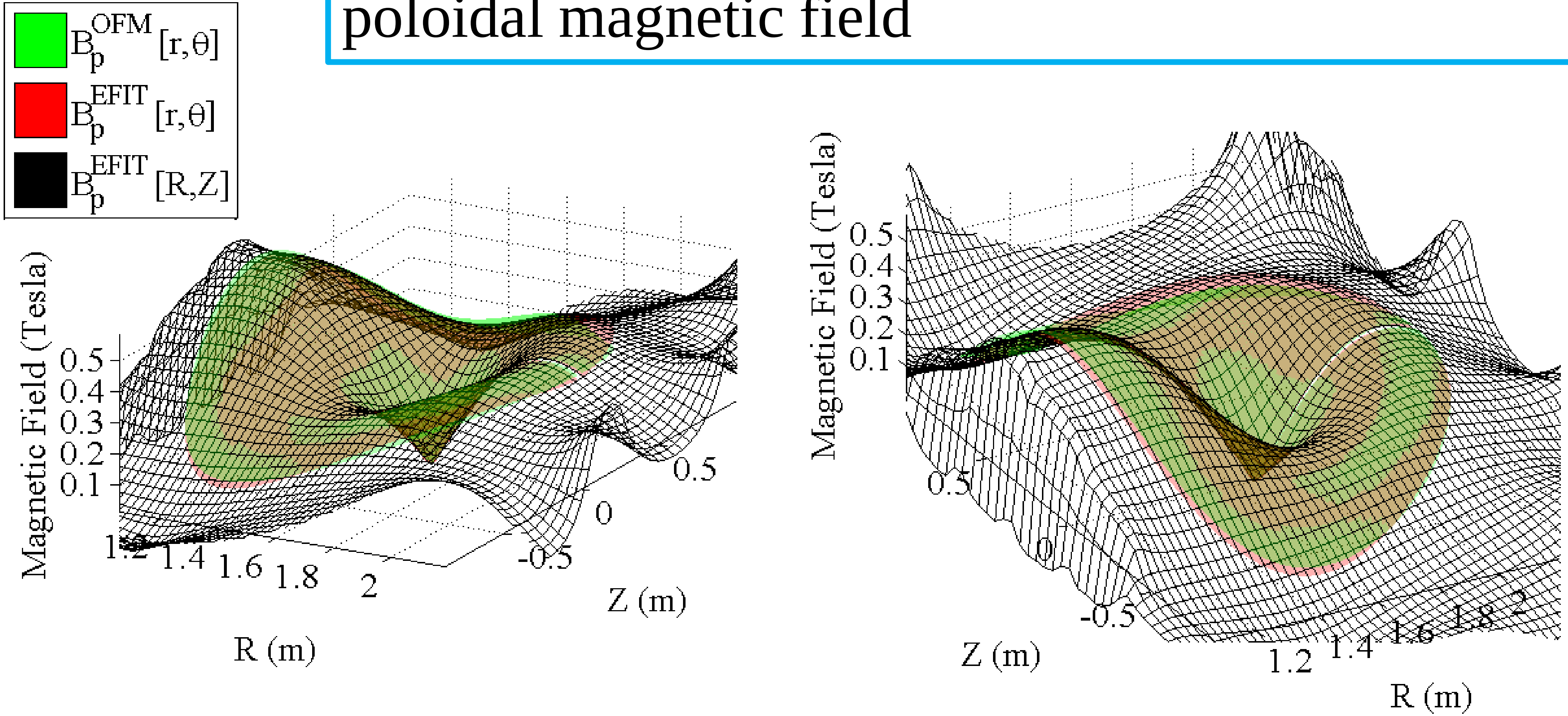

- The poloidal magnetic field directly calculated from the raw EFIT (R,Z) data using **(2)** is shown as the black mesh. The same data, interpolated onto flux-surfaces, is shown in red.
- The results of **(3)**, at the Orthogonalized Fitted Miller (OM, or OFM) coordinate system locations, using gradients in the direction of the OM basis vectors, is shown in green

The poloidal dependence of plasma properties can be represented by low-order Fourier expansions

- The poloidal dependence of the plasma density, electric potential, and components of the velocity can be modeled using 1st order Fourier expansions. These expansions express the poloidally-dependent quantity in terms of the "average" quantity $\bar{x}_\alpha$, and sine and cosine asymmetries O(r/R)

$$x_\alpha[r,\theta] = \bar{x}_\alpha[r]\left(1 + x_\alpha^s[r]\sin[\theta] + x_\alpha^c[r]\cos[\theta]\right)$$

- For shot 149468, radial measurements of deuterium and carbon rotation velocities are available, along with density and temperature calculations.

$$\left\{\bar{n}_d, \bar{n}_c, \bar{V}_{\phi,d}, \bar{V}_{\phi,c}, \bar{V}_{\theta,d}, \bar{V}_{\theta,c}, \bar{\Phi}\right\}$$

- Sine and cosine moments of the plasma fluid equations can be used to formulate a system of equations to solve for the poloidal asymmetries

$$\left\{n_d^s, n_d^c, n_c^s, n_c^c, V_{\phi,d}^s, V_{\phi,d}^c, V_{\phi,c}^s, V_{\phi,c}^c, V_{\theta,d}^s, V_{\theta,d}^c, V_{\theta,c}^s, V_{\theta,c}^c, \Phi^s, \Phi^c\right\}$$

- The moments of the continuity equation are used to determine the density asymmetries (4 equations), the poloidal momentum balance moments used for the asymmetries in poloidal velocity (4 equations), and the toroidal angular momentum balance moments are applied to find the asymmetries in toroidal velocity (4 equations). Charge neutrality, coupled with the moments of the poloidal momentum balance for electron species, is used to relate the density asymmetries to the asymmetries in electric potential.

The flux-surface-averages of the Fourier moments of the continuity and momentum balance equations can be formulated using OM coordinate scale factors[7,8]

$$\boxed{z_n = \{\sin[\theta], \cos[\theta]\}}$$

- Continuity

$$\left\langle z_n \left(\vec{V}_i \cdot \nabla n_i + n_i \nabla \cdot \vec{V}_i \right) \right\rangle = \left\langle z_n S_i^0 \right\rangle$$

- Radial force balance

$$\left\langle z_n \frac{1}{h_\rho} \frac{\partial P_i}{\partial \rho} \right\rangle = \left\langle z_n n_i e_i \left(-\frac{1}{h_\rho} \frac{\partial \Phi}{\partial \rho} + V_{\theta i} B_\phi - V_{\phi i} B_\theta \right) \right\rangle$$

- Poloidal force balance

$$\left\langle z_n \left[m_i \nabla \cdot \left(n_i \vec{V}_i \vec{V}_i \right) \right]_\theta \right\rangle + \left\langle z_n \frac{1}{h_\theta} \frac{\partial P_i}{\partial \theta} \right\rangle + \left\langle z_n \left[\nabla \cdot \overleftrightarrow{\Pi}_i^0 \right]_\theta \right\rangle + \left\langle z_n \left[\nabla \cdot \overleftrightarrow{\Pi}_i^{34} \right]_\theta \right\rangle = \left\langle z_n n_i e_i \left(E_\theta - V_{ri} B_\phi \right) \right\rangle + \left\langle z_n F_{\theta i}^1 \right\rangle + \left\langle z_n S_{\theta i}^1 \right\rangle$$

- Toroidal angular momentum balance

$$\left\langle z_n R \left[m_i \nabla \cdot \left(n_i \vec{V}_i \vec{V}_i \right) \right]_\phi \right\rangle + \left\langle z_n R \left[\nabla \cdot \overleftrightarrow{\Pi}_i^0 \right]_\phi \right\rangle + \left\langle z_n R \left[\nabla \cdot \overleftrightarrow{\Pi}_i^{34} \right]_\phi \right\rangle = \left\langle z_n R n_i e_i \left(E_\phi^A + V_{ri} B_\theta \right) \right\rangle + \left\langle z_n R F_{\phi i}^1 \right\rangle + \left\langle z_n R S_{\phi i}^1 \right\rangle$$

The flux-surface-average (FSA) of a poloidally dependent quantity C[θ] is defined as:

$$\langle C[\theta] \rangle = \frac{\int_0^{2\pi} C[\theta]\, H_{r\theta} R \,\mathrm{d}\theta}{\int_0^{2\pi} H_{r\theta} R \,\mathrm{d}\theta} = \frac{\int_0^{2\pi} C[\theta] \frac{h_\theta \mathrm{d}\theta}{B_\theta}}{\int_0^{2\pi} \frac{h_\theta \mathrm{d}\theta}{B_\theta}}$$

Calculation of poloidal asymmetries of plasma properties

- A direct-substitution method, formulated using Mathematica and ported to Fortran for execution, can be used to solve the coupled set of 14 nonlinear equations for the asymmetries in plasma parameters at 50 radial meshes.
- The resulting radial profiles can be used with the experimental mean-values of plasma parameters to reconstruct the poloidal variations of plasma density, velocity, and electric field across a plasma cross-section.

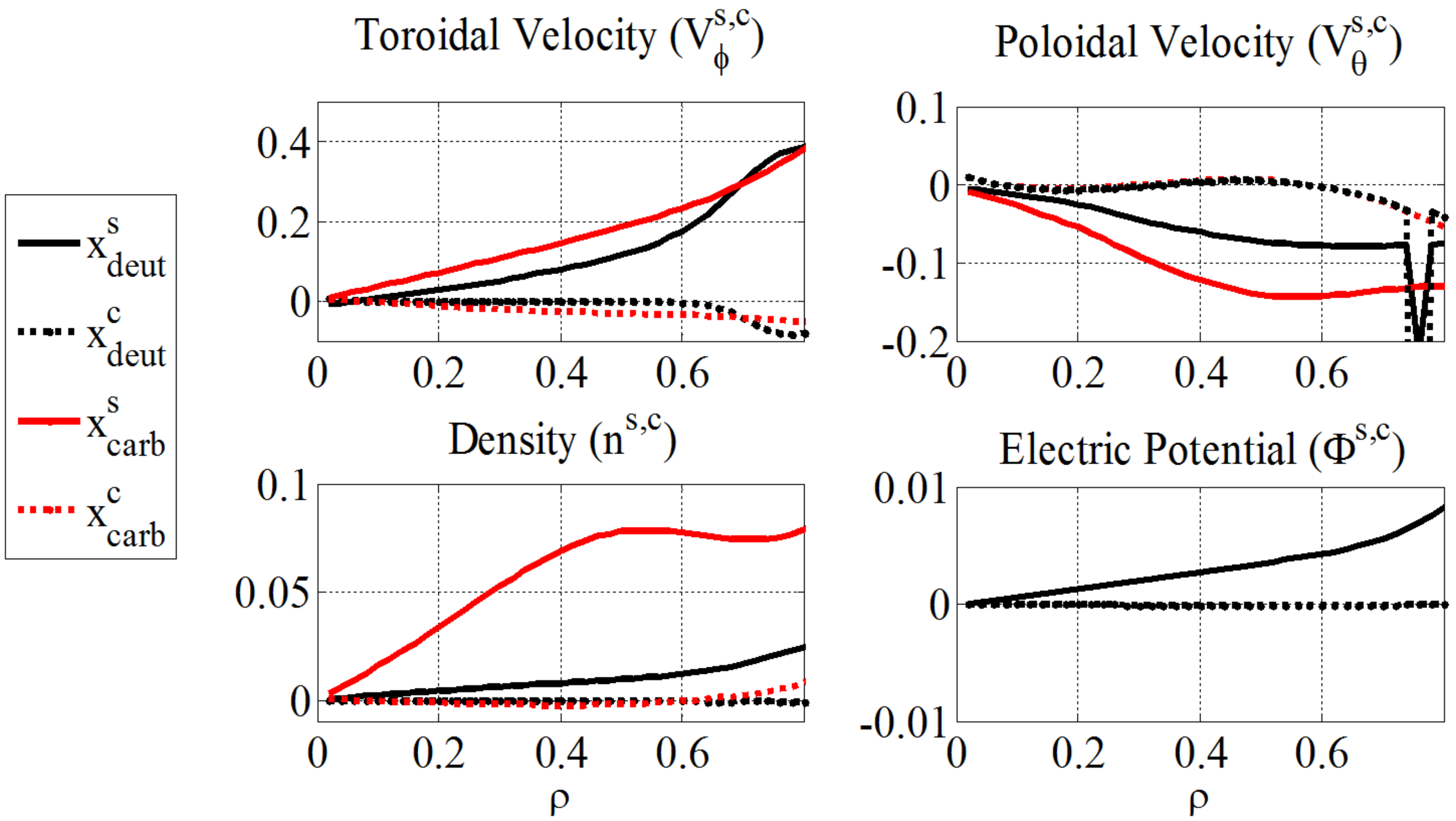

Figure – The calculated radial profiles of sine and cosine asymmetries for Shot# 149468, t=1900.5 ms

Calculations of poloidally asymmetric density and toroidal velocity distributions

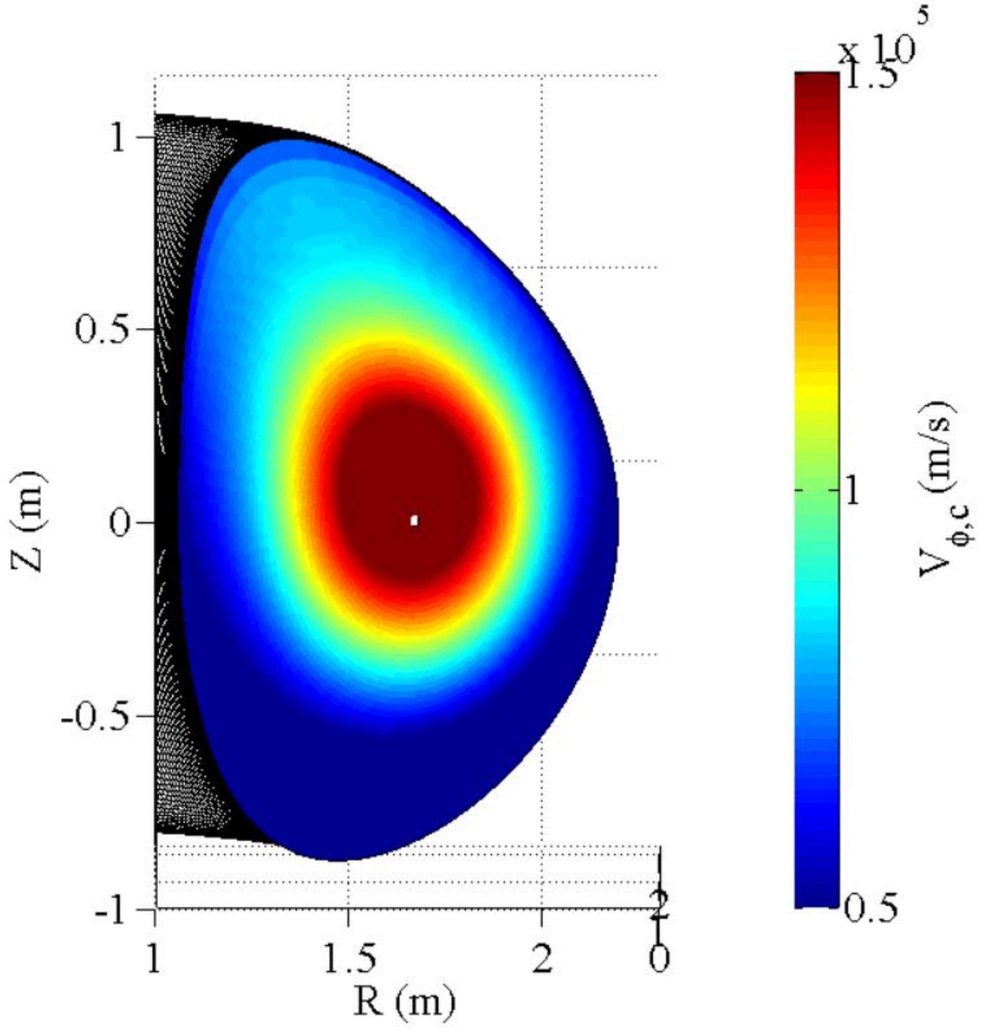

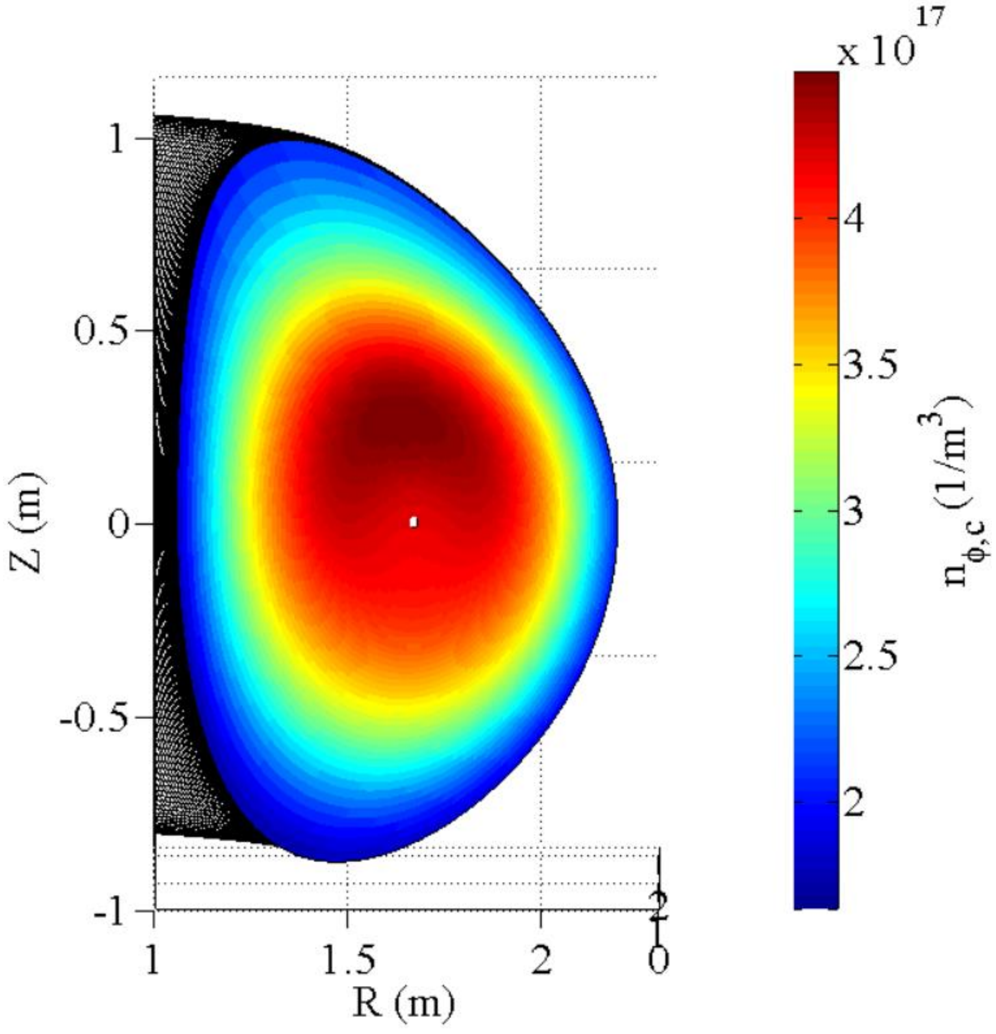

Left Figure – Carbon toroidal velocity, accounting for the calculated poloidal asymmetries

Right Figure – Carbon density, accounting for the calculated poloidal asymmetries

Conclusions

- The agreement of the traditional Miller plasma model with EFIT predictions for flux-surface locations can be significantly improved if its fit-parameters are evaluated separately between the upper/lower hemispheres. The accuracy of the resulting extended-Miller geometric model is comparable to 6th order Fourier expansions of minor radius, with errors less than 0.5% for $\rho<0.9$, while requiring half the number of fitting coefficients.

- Poloidal magnetic fields calculated in orthogonalized forms of general fitted non-orthogonal geometric models, such as the extended-Miller, agree with traditional Cartesian coordinate calculations of the magnetic field from EFIT data to within 5% for $\rho<0.8$.

- Poloidal variations from experimental plasma densities, velocities, and electric potential can be calculated by solving Fourier sine and cosine moments of the plasma fluid equations for poloidal asymmetries in orthogonalized extended Miller geometry

Future work

- Use a higher-order Fourier expansion to represent the poloidal asymmetries
- Apply the r-Fourier method to the fluid calculations as an alternative to the Miller model. This should allow for analytic calculations of the flux-surface-averages, and allow for an analysis of how much error is due to low-order Fourier expansions
- Consider the effects of toroidal asymmetries on toroidal drag, and compare with experiment

Extra - RZ-Fourier model flux surface location interpolation and fitting, and basis vector calculations

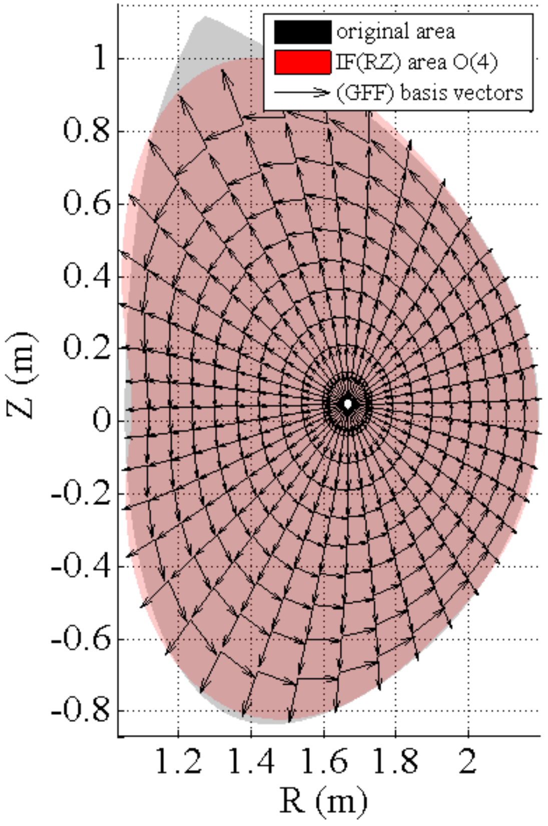

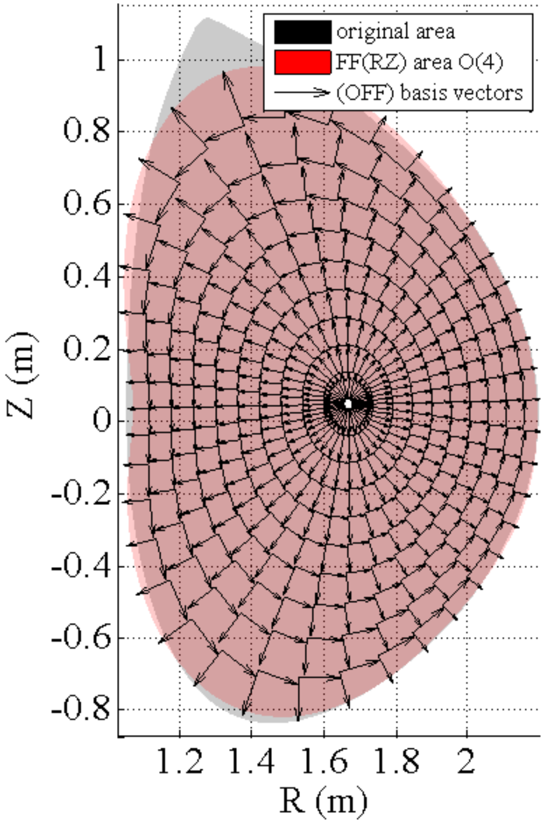

This parameterization requires 4n + 2 = 18 radial profiles, and radial gradients:

$$\left\{\bar{R}[\rho],\bar{Z}[\rho],R_i^s[\rho],R_i^c[\rho],Z_i^s[\rho],Z_i^c[\rho]\right\}$$

Reconstruction of the plasma area from two seperate 4th order Fourier fits of the poloidal dependence of EFIT major radius R and vertical displacement Z (blue), as compared to the original EFIT plasma area (grey).

Left Plot:

Interpolated Fourier RZ (IFRZ) – Independent poloidal interpolation of Fourier fit coefficients on each flux surface (red)

General Fitted Fourier (GFFRZ) – General, non-orthogonal basis vectors

Right Plot:

Fitted Fourier RZ (FFRZ) – reconstruction from 4th order, piecewise polynomial fits of the radial dependence of Fourier fit coefficients

Orthogonalized Fitted Fourier (OFFRZ) – orthogonalized basis vectors

Extra - Formulating the Toroidal Angular Momentum Balance in terms of drag frequencies

- The toroidal angular momentum balance can be written in terms of a drag frequency, which describes all physical processes contributing to toroidal angular momentum which are not well understood:

$$m_i \bar{n}_i \bar{V}_{\phi i} R_0 \nu^*_{d\phi i} = \langle R n_i e_i \left(E^A_\phi + V_{ri} B_\theta \right) \rangle + \langle R F_{\phi i} \rangle + \langle R S^1_{\phi i} \rangle \qquad \textbf{(4)}$$

- In the center of the plasma, where charge-exchange effects are small, the drag frequency is dependent on the inertial and gyroviscous effects. This drag frequency can be used with **(4)** to predict a toroidal velocity, consistent with the 0th moment of the toroidal angular momentum balance

$$\nu^*_{d\phi i} \approx \left(\nu^*_{d\phi i} \right)_{calc} = \left(\nu^*_{d\phi i} \right)_{inert} + \left(\nu^*_{d\phi i} \right)_{\Omega}$$

$$\left(\nu^*_{d\phi i} \right)_{inert} = \frac{1}{R_0 \bar{n}_i m_i \bar{V}_{\phi i}} \left\langle R n_i m_i \left[\left(\vec{V}_i \cdot \nabla \right) \vec{V}_i \right]_\phi \right\rangle$$

$$\left(\nu^*_{d\phi i} \right)_{\Omega} = \frac{1}{R_0 \bar{n}_i m_i \bar{V}_{\phi i}} \left\langle R \left(\nabla \cdot \overleftrightarrow{\Pi}^{34}_i \right)_\phi \right\rangle$$

$$\boxed{\bar{V}^{calculated}_{\phi i} = \frac{\langle R n_i e_i \left(E^A_\phi + V_{ri} B_\theta \right) \rangle + \langle R n_i m_i \nu_{iI} V_{\phi I} \rangle + \langle R S^1_{\phi i} \rangle}{m_i \bar{n}_i R_0 \nu^*_{d\phi i} + \langle R n_i m_i \nu_{iI} \left(1 + V^s_{\phi i} \sin[\theta] + V^c_{\phi i} \cos[\theta] \right) \rangle}}$$

- Work is ongoing to determine the effects that the calculations of poloidal asymmetries will have on the values of $\left(\nu^*_{d\phi i} \right)_{\Omega}$ and $\bar{V}^{calculated}_{\phi i}$

Extra – Comparison of inferred and calculated drag frequencies

- The inferred drag frequencies are negative, opposite the direction of the calculated drag. If true, this indicates a much larger, unmodeled toroidal drag, possibly due to parallel viscosity due to toroidal axisymmetries

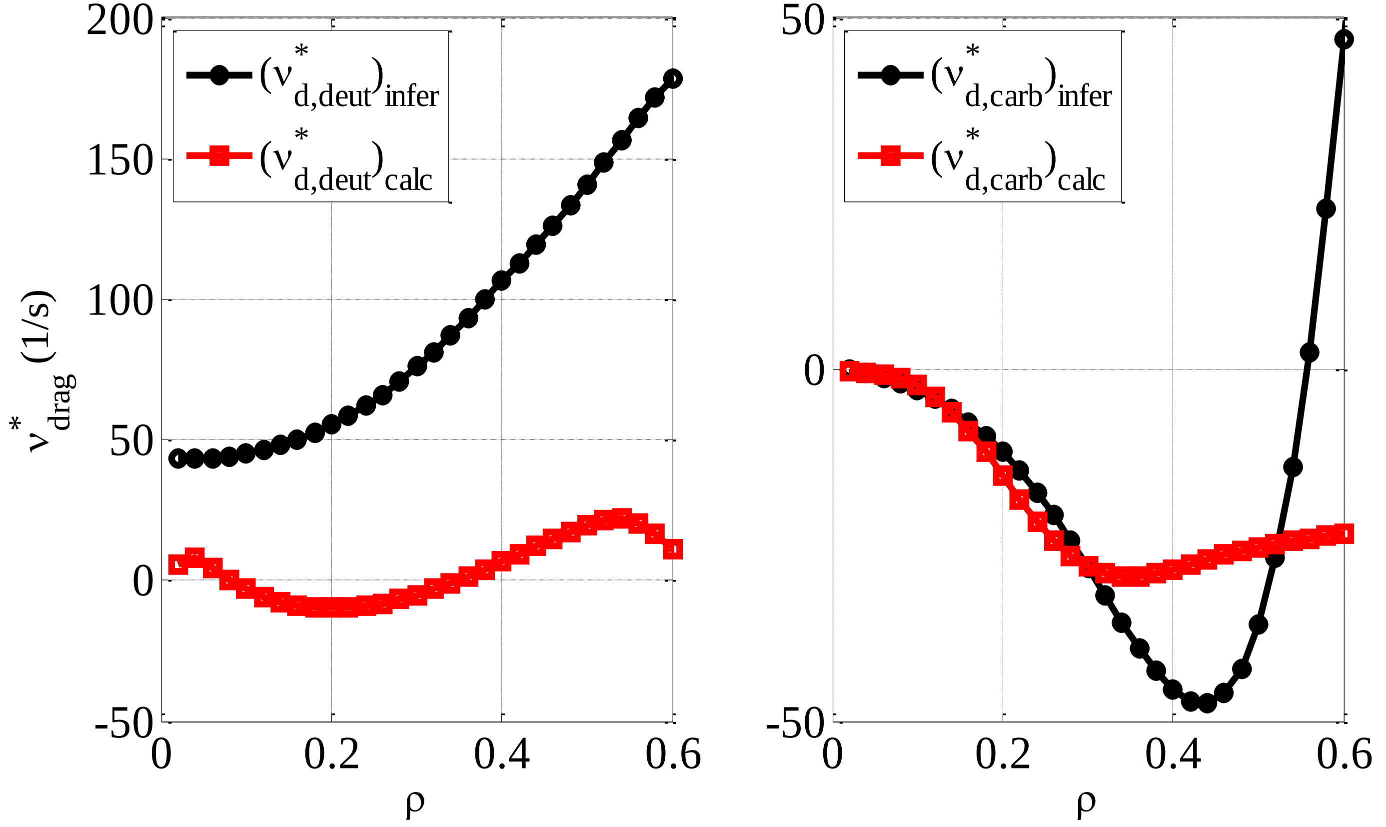

Extra – Velocity predictions using calculated drag frequencies

- The toroidal angular momentum balance equations for deuterium and carbon can be reformatted to calculate toroidal velocity in terms of the drag frequencies calculated from gyroviscous theory

$$\bar{V}_{\phi i}^{calculated} = \frac{\langle R n_i e_i \left(E_\phi^A + V_{ri} B_\theta\right)\rangle + \langle R n_i m_i \nu_{iI} V_{\phi I}\rangle + \langle R S_{\phi i}^1\rangle}{m_i \bar{n}_i R_0 \nu_{d\phi i}^* + \langle R n_i m_i \nu_{iI}\left(1 + V_{\phi i}^s \sin[\theta] + V_{\phi i}^c \cos[\theta]\right)\rangle}$$

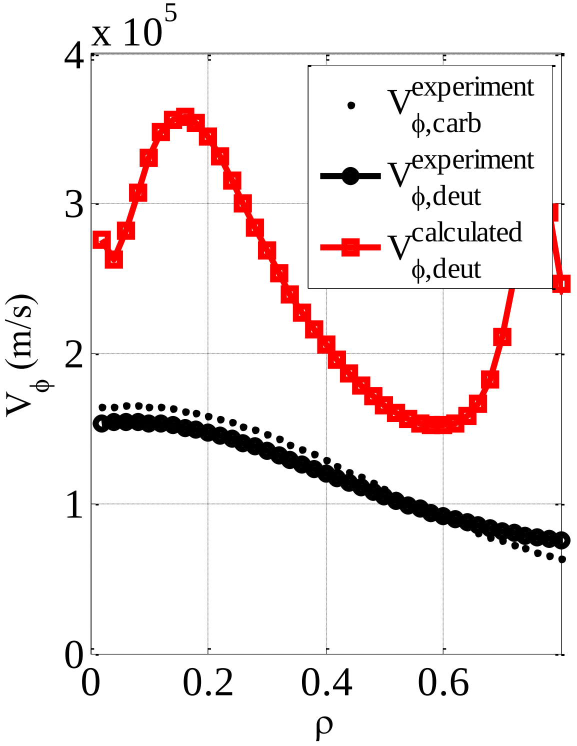

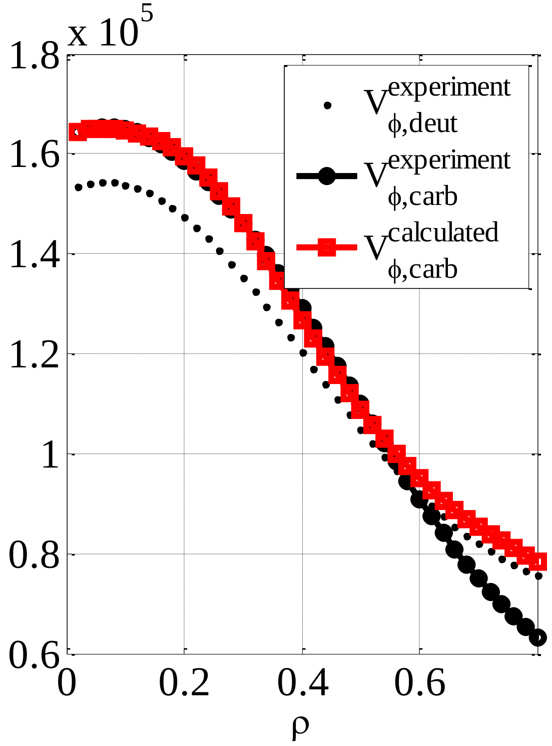

Extra – more detailed friction

- The forces due to friction on particle species α due to interactions with a velocity distribution of species β can be represented in terms of an interspecies collision frequency:

$$F_\alpha^1 = \frac{\partial p_\alpha}{\partial t} = -n_\alpha m_\alpha \left(V_\alpha - V_\beta\right)\nu_{\alpha,\beta}$$

- Where the collision frequency is [1]:

$$\bar{\nu}_{\alpha,\beta} = \frac{1}{6\sqrt{2}\,\pi^{3/2}\epsilon_0^2}\frac{n_\beta e_\alpha{}^2 e_\beta{}^2\sqrt{\mu_{\alpha,\beta}}\,ln\Lambda}{m_\alpha T^{3/2}}$$

- In a two-species deuterium-carbon plasma, this form ensures that the frictional forces between species sum to zero

$$F_c^1 = n_c m_c \left(V_c - V_d\right)\nu_{c,d} = n_d m_d \left(V_d - V_c\right)\nu_{d,c} = F_d^1$$

Extra – more Miller comparison plots

Miller, interpolated and fitted (black), vs. EFIT (red)

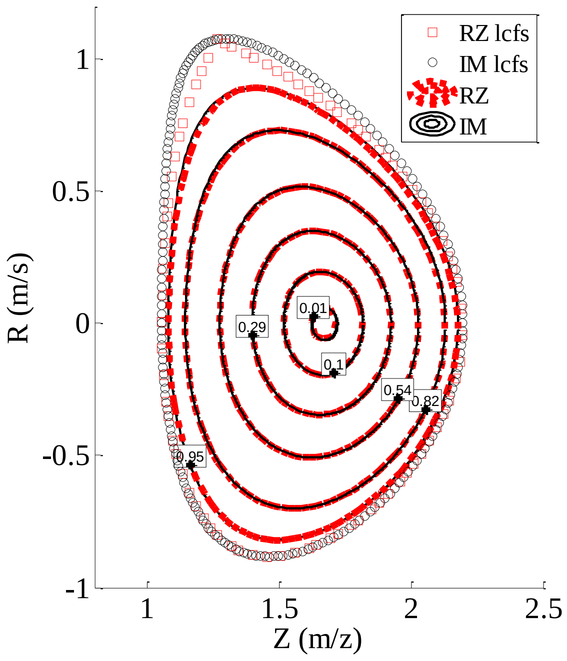

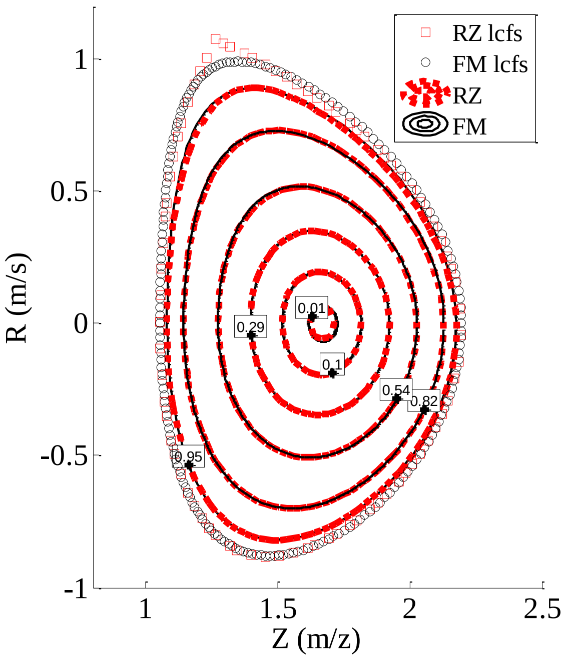

Angle between fitted and interpolated miller

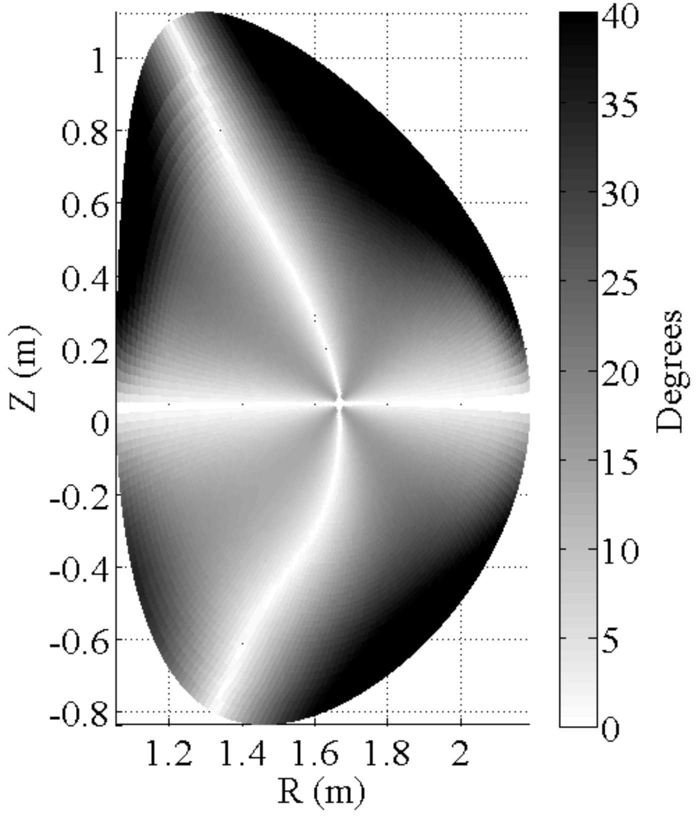

Traditional Miller flux-surface fits and error

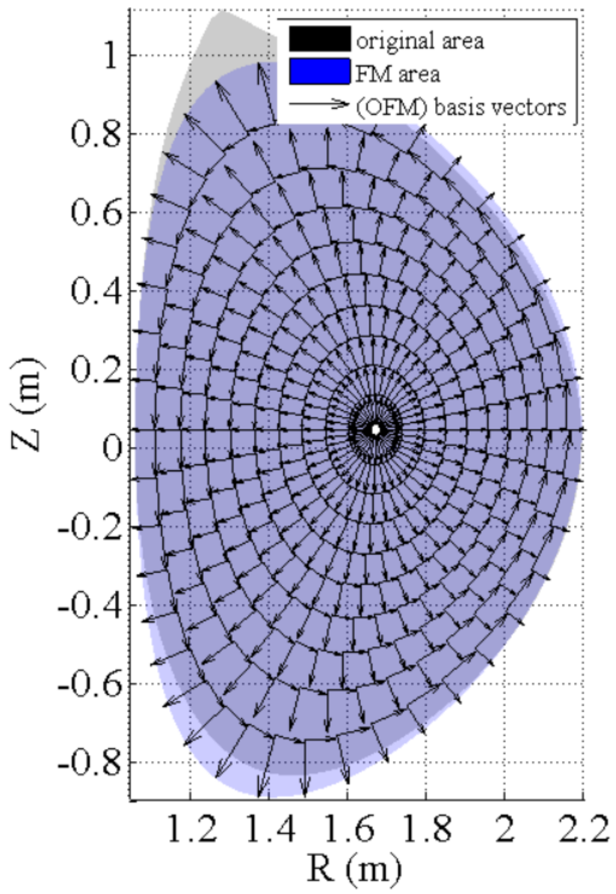

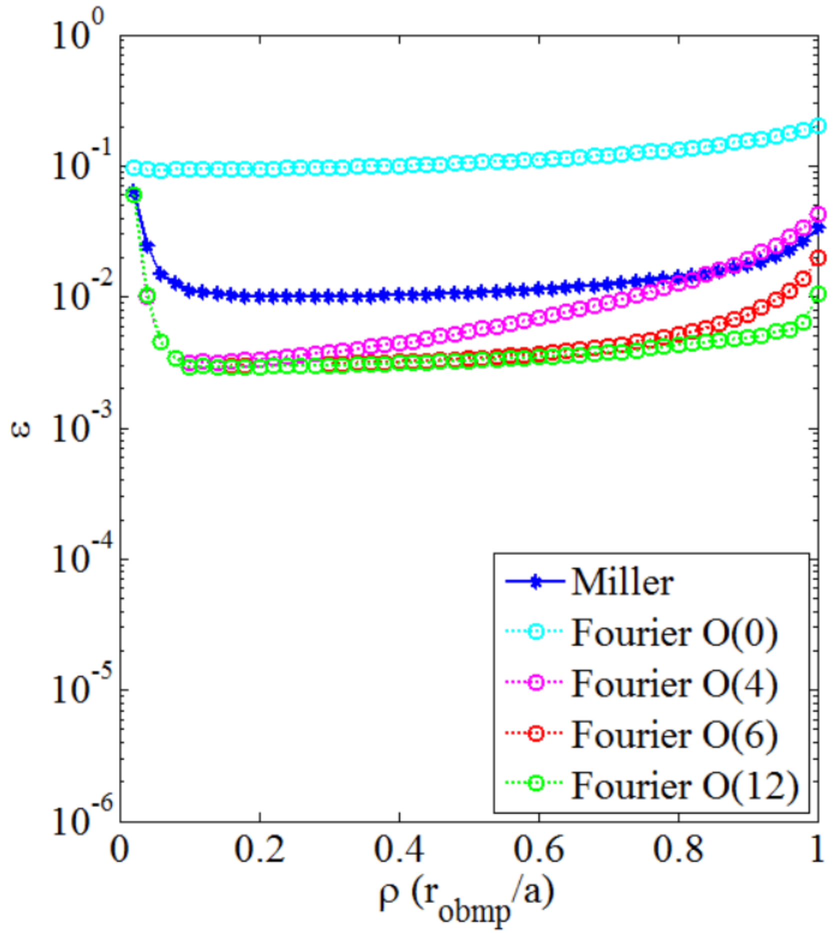

The error associated with the traditional Miller model for shot 149468, using a uniform triangularity and elongation between the upper and lower hemispheres, is ~ 1% for <0.9, and ~ 3% in the very edge.

This is fairly consistent with the calculations performed by Candy [6]

Left Figure:
Original EFIT plasma area (grey), fitted traditional Miller plasma area (blue), and orthogonalized traditional Miller basis vectors

Right Figure:
Error between the traditional-Miller flux-surface fits (blue), and various orders of Fourier fitting, as compared to the EFIT data. Error calculated using the method described on slide # 13